JOURNAL OF MATERIALS SCIENCE 37 (2002) 3045–3051

Synthesis of ferroelectric $Sr_xBa_{1-x}Nb_2O_6$ bulk ceramics, thin film and multi-layered film

KEN-ICHI KAKIMOTO
Department of Material Science and Engineering, Faculty of Engineering, Nagoya Institute of Technology, Gokiso-cho, Showa-ku, Nagoya 466-8555, Japan
E-mail: kakimoto@mse.nitech.ac.jp

H. KAKEMOTO
Department of Metallurgy and Ceramic Science, Graduate School of Science and Engineering, Tokyo Institute of Technology, 2-12-1 Ookayama, Meguro-ku, Tokyo 152-8552, Japan

A. BABA, S. FUJITA, Y. MASUDA
Department of Electrical and Electronic Engineering, Faculty of Engineering, Hachinohe Institute of Technology, 88-1 Oobiraki, Myo, Hachinohe, Aomori 031-8501, Japan

1. Introduction

Strontium barium niobate $Sr_xBa_{1-x}Nb_2O_6$ (SBN, $0.25 < x < 0.75$) is believed to be a solid solution in the $SrNb_2O_6$-$BaNb_2O_6$ pseudobinary system [1] and exhibits a crystal structure closely related to the tetragonal tungsten bronze structure (4 *mm*) with a unit-cell formula of $[(A1)_4(A2)_2C_4B_{10}O_{30}]$ [2]. This structure consists of a framework of NbO_6 octahedra including different types of interstitial sites: A1 site for a coordination number of 15, A2 site of 12, C site of 9 and B site of 6. Two of such interstitial sites A1 and A2 are generally occupied by Sr/Ba cations, while the C site is vacant. However, Sr/Ba cations in actual SBN materials are considered to be not distributed regularly at those sites, but seem to form various local coordinations depending on the x value.

SBN is well known in particular that it exhibits an extremely high electro-optic coefficient [3] and strong photorefractive effects [4, 5], since the crystal is transparent over a wide length wave range. Further, SBN should demonstrate excellent ferroelectric properties due to the fact that spontaneous polarization occurs along the c-axis of the tetragonal structure and the Curie point can be continuously shifted in the range from 50 to 250°C by controlling the x value [6]. However, the number of studies on the dielectric and ferroelectric properties of SBN is quite limited, resulting in a lack of knowledge of their properties still.

Various fabrication techniques can be used for the synthesis of SBN. The methods reported so far include the Czochralski method for single crystals [7], solid-state sintering by hot pressing [8], hot isostatic pressing [9] for bulk ceramics, and liquid phase epitaxy [10], sol-gel synthesis [11], rf magnetron sputtering [12] and pulsed laser deposition (PLD) [13–15] for thin films.

In particular, ferroelectric thin films are rapidly gaining importance as promising candidate materials for application to nonvolatile ferroelectric random access memory (FeRAM) as well as micro active components, e.g., accelerometers, sensors and actuators. To date, ferroelectric thin films like Pb(Zr, Ti)O_3 (PZT) of perovskite structure and $SrBi_2Ta_2O_9$ (SBT) of Bi-layered perovskite structure have been most extensively studied for their applications. In addition, it should be noted that the number of reports on the preparation of such ferroelectric thin films by PLD method has increased remarkably in recent years. One of the most important advantages of employing PLD to synthesize oxide thin films is the fact that the composition is easily transferred from the sintered bulk target to the deposited film, since the film deposition can be carried out under an ambient of the desired pressure, even for an oxidising atmosphere. The reason is that there is no source in the deposition chamber, but a short-wavelength pulsed laser is focused onto the target material through a chamber window from an external laser generator. Excimer lasers, e.g., KrF ($\lambda = 248$ nm) and XeCl ($\lambda = 308$ nm) are often used for the laser source of PLD [13–15]. On the other hand, $Nd^{3+}:Y_3Al_5O_{12}$ (YAG) laser has superior advantages in running costs, easy maintenance and safety compared to excimer lasers. While YAG laser generates $\lambda = 1064$ nm as a standard wavelength, it can generate a shorter wavelength of $\lambda = 266$ nm (the fourth harmonic generation, FHG) using nonlinear optical crystals (KH_2PO_4, KDP). A shorter wavelength is expected to give a higher average power transmission suitable for PLD.

In the present study, SBN bulk ceramics with various x values were fabricated through a conventional mixed-oxide route, and then the PLD technique by FHG-YAG was applied for the preparation of SBN thin films from selected bulk targets. Microstructure and ferroelectric, properties of SBN bulk and thin films were investigated. Also we tried to prepare multi-layered SBN films from the target sources with different x values in order to control the temperature-dependence of the dielectric constant of thin films.

2. Experimental procedure

The raw materials used in this experiment were high-purity powders of $SrCO_3$ (Kanto Chemical

0022–2461

Co., 99.6%), $BaCO_3$ (Shin Nippon Chemical Co., 99.97%) and Nb_2O_5 (Kanto Chemical Co., 99.95%). All compositions were prepared in accordance with the formula $xSrCO_3 + (1-x)\ BaCO_3 + Nb_2O_5 = Sr_xBa_{1-x}Nb_2O_6 + CO_2$, where x varies from 0 to 1.0 at 0.1 intervals. The mixed powders were transferred to a polyethylene mill jar containing partially stabilized ZrO_2 (PSZ) balls and milled for 24 h in methanol. The thick slurry was dried completely in an infrared oven at 100°C within approximately 5 h. The dried material was crushed and sieved, followed by uni-axial pressing at 100 MPa into cylindrical forms of diameter 20 mm and height 5 mm. The green tablets were calcined at 1000°C for 10 h in an Al_2O_3 crucible and crushed by ball-milling, followed by forming and sintering at 1250°C for 10 h. The crystal phases were identified by X-ray diffraction (XRD, Rigaku RAD3C) using Cu K_α radiation. Density was determined from the weight and dimensions, and compared with the density calculated from the lattice parameters that were determined by XRD data.

SBN thin films were deposited using the PLD technique. A YAG laser beam (Spectron Laser System SL850) with a wavelength of $\lambda = 266$ nm (FHG) and a repetition rate of 10 Hz was focused on to rotating, sintered SBN targets. The flux of the incident laser beam on to the target was varied from 0.9 to 3.2 J/cm^2 and the base pressure of the vacuum chamber was in the 10^{-5} Pa range. Films were deposited on quartz or Pt-coated Si substrates heated in the temperature range from 500 to 700°C, under an oxygen partial pressure ambient of 1 to 9 Pa, followed by thermal annealing at 800°C under an oxygen atmosphere. The films were analyzed by XRD, X-ray fluorescence spectroscopy (XRF, Rigaku 3030) and atomic force microscopy (AFM, Digital Instruments Nano Scope III). A surface roughness micrometer measured film thickness. For electrical measurements, an Au top electrode was sputtered on the film/Pt/Si specimens using a contact mask with multiple holes (ϕ1 mm). The dielectric properties were measured at room temperature in the frequency range from 1 to 100 kHz using an LCR meter (HP 4284A). Further, the temperature dependence of dielectric constant ε_r and dielectric loss (tan δ) at 1 kHz was investigated at elevated temperatures of up to 350°C. Ferroelectric D–E hysteresis loops were observed using a modified Sawyer-Tower circuit.

3. Results and discussion

3.1. SBN bulk ceramics

SBN bulk specimens showed relatively good sintering behaviors without coarse grains and large pores, and exhibited densities of 84–95% of their theoretical maximum values (Fig. 1). XRD measurements indicated that those SBN bulk specimens with x values from 0.3 to 0.7 showed a single tetragonal phase (Figs 1 and 2a), while the specimens with higher Sr contents over $x = 0.7$ additionally contained small amounts of orthorhombic strontium niobate phases. Fig. 3 shows the temperature dependence of ε_r and tan δ measured

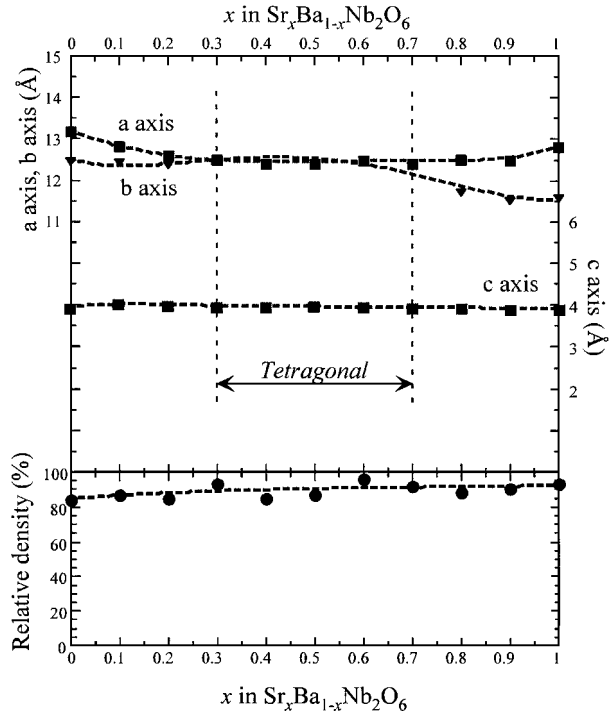

Figure 1 Changes in lattice parameters and density for $Sr_xBa_{1-x}Nb_2O_6$ bulk specimens.

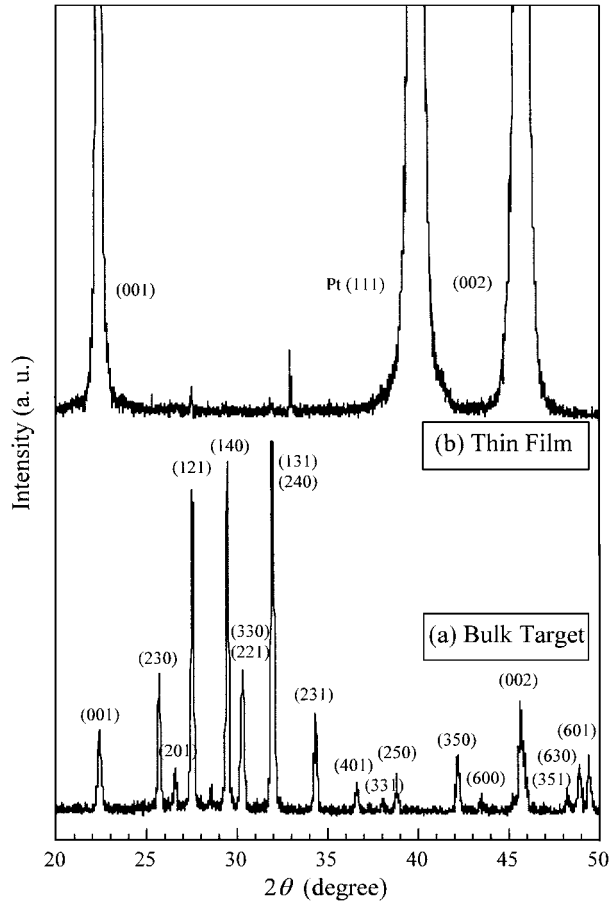

Figure 2 XRD patterns of (a) sintered $Sr_{0.3}Ba_{0.7}Nb_2O_6$ bulk specimen and (b) its thin film prepared by PLD.

at 1 kHz for several SBN bulk specimens. The Curie point (T_c), which corresponds to the peak position of ε_r shifts to lower temperatures with increasing x value, which may be caused by different local configurations

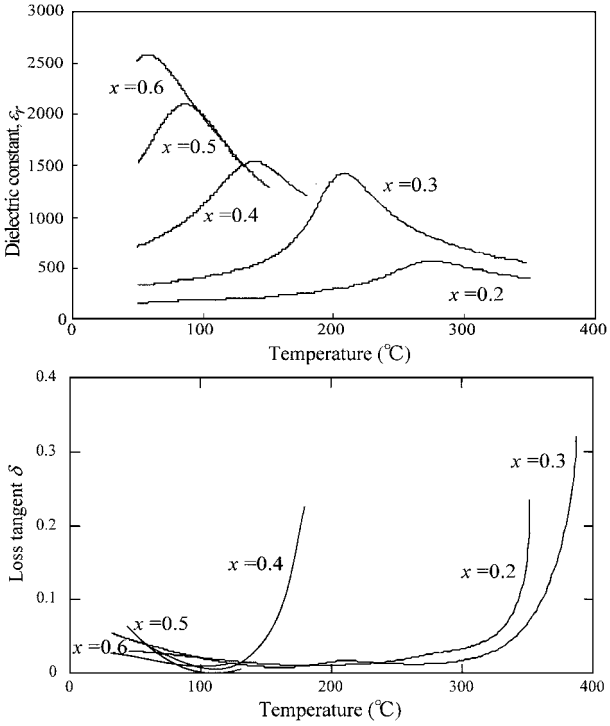

Figure 3 Temperature dependence of dielectric constant ε_r and loss tangent (tan δ) measured at 1 kHz for $Sr_xBa_{1-x}Nb_2O_6$ bulk specimens with x from 0.2 to 0.6.

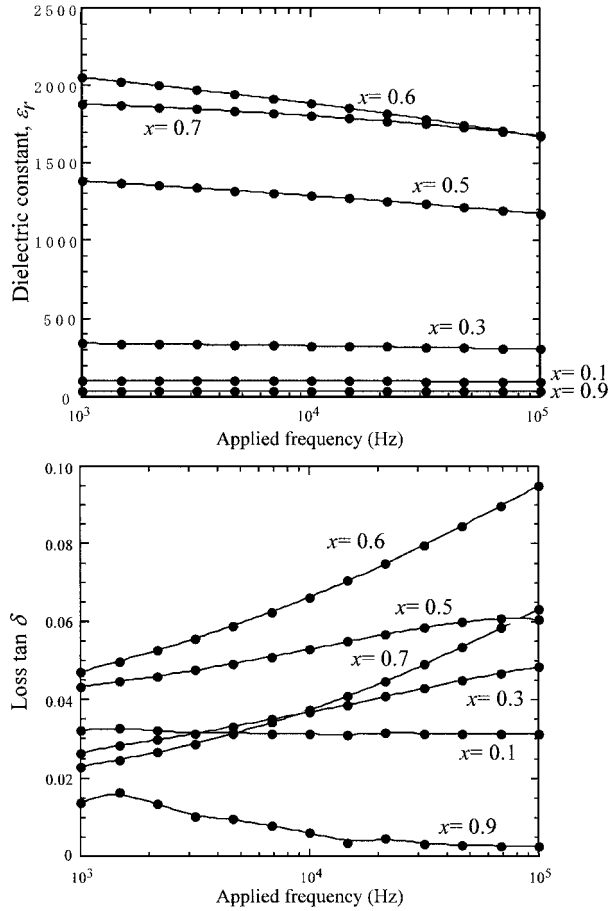

Figure 4 Frequency dependence of dielectric constant ε_r and loss tangent (tan δ) measured at room temperature for $Sr_xBa_{1-x}Nb_2O_6$ bulk specimens with x from 0.1 to 0.9.

in the tetragonal tungsten bronze (TTB) structure [16]. T_c varies widely from 275°C for $x = 0.2$ to 58°C for $x = 0.6$. A similar T_c variation with SBN composition has been reported both for single crystals [6, 17] and polycrystals [9]. In addition to the configuration effect, VanDamme *et al*. [9] discussed such a T_c variation from a viewpoint of microstructural differences, e.g., grain size and its uniformity for the polycrystalline SBN specimens. They compared several specimens prepared by pressure less sintering at different temperatures and post-HIP treatment. The specimens showed different TTB crystallinities and grain sizes, which resulted in a T_c variation in spite of the same SBN composition. Therefore, synergic effects due to compositional and microstructural differences seem to appear in the temperature dependence of ε_r for polycrystalline SBN bulk ceramics. On the other hand, the maximum values of ε_r shown in Fig. 3 are much smaller than those for single crystals because of less preferential orientation in crystallinity, but they increase with increasing x value. Tan δ at the Curie point remains at 0.03 or less for SBN specimens with x of 0.2–0.6. In particular, tan δ of the specimens with x of 0.2 and 0.3 remains 0.02 up to 300°C and exhibits only a slight increase from 0.026 at 1 kHz to 0.048 at 100 kHz at room temperature, as shown in Fig. 4 ($x = 0.3$). The other TTB-structured specimens show much larger values of tan δ in the measurements at elevated temperatures and at various frequency levels from 1 to 100 kHz.

Fig. 5 shows the electrical polarization–electrical field (P–E) hysteresis loops recorded at room temperature for the SBN specimens with x values from 0 to 1.0. The estimated remanent polarization (P_r) and coercive field (E_c) are summarized in Fig. 6. The SBN specimens with x of 0, 0.8, 0.9 and 1.0 show linear P–E relationships, and no P_r and E_c are observed. In contrast, the SBN specimens with x of 0.2 to 0.7 demonstrate ferroelectric P–E hysteresis loops, but an ellipsoidal shape is observed for $x = 0.2$ while typical rhomboidal shapes appear for the other specimens. P_r shows a maximum peak of 1.65 μC/cm^2 at $x = 0.5$, and E_c decreases with increasing x value in the ferroelectric TTB-structured region.

It is evident from the above results that the TTB-structured SBN bulk specimens with x of 0.3–0.6 have superior ferroelectric properties to the others, in that they showed rhomboidal P–E hysteresis loops with relative high P_r and low E_c values. These SBN bulk specimens were selected as target sources for synthesizing SBN thin films and multi-layered films by the PLD method.

3.2. SBN thin films

Prior to deposition on Si-based substrates, quartz substrates were used for investigating the influence of PLD conditions on the characteristics of SBN thin films. SBN bulk ceramics with x of 0.3 were used as target sources for this experiment. When PLD was employed under an oxygen partial pressure (P_{O_2}) of 5 Pa at a substrate temperature (T_{sub}) of 700°C, increasing flux of the incident laser beam on to the target from 0.9 to 3.2 J/cm^2 enhanced a film deposition rate from 5.8 to 23.5 nm/min. It was also found that a single TTB

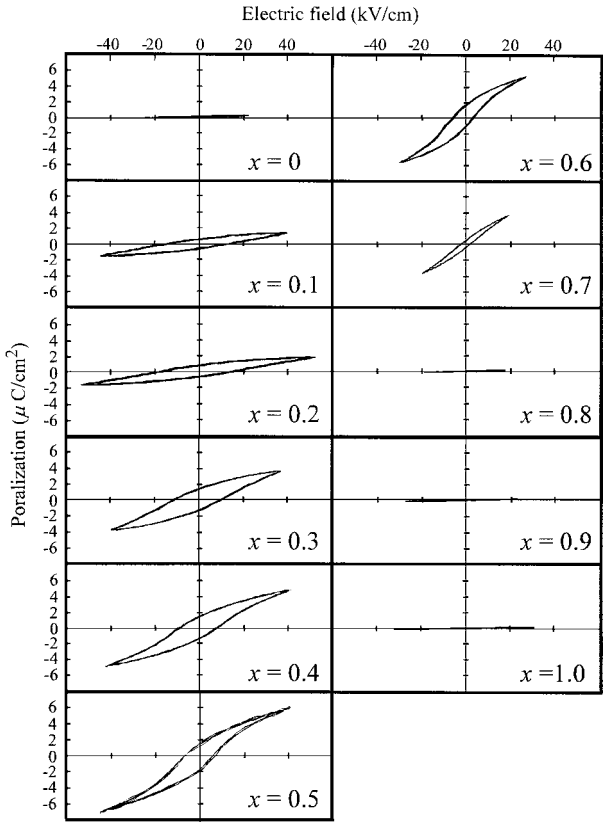

Figure 5 Electrical polarization–electrical field (P–E) hysteresis loops recorded at room temperature for $Sr_xBa_{1-x}Nb_2O_6$ bulk specimens with x from 0 to 1.0.

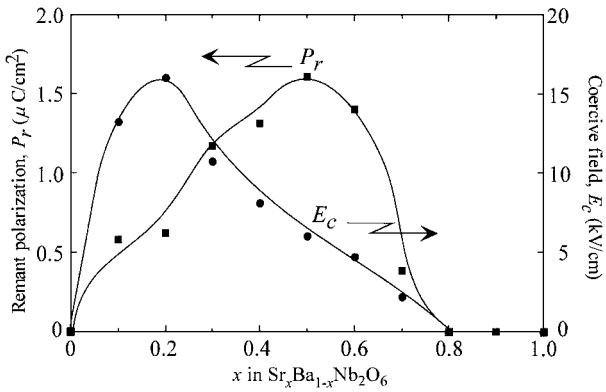

Figure 6 Remanent polarization P_r and coercive field E_c observed in Fig. 5.

phase became dominant above 2.1 J/cm^2. In particular, the TTB phase started to appear at higher T_{sub} values above 650°C. The deposited SBN thin film showed almost the same cation composition as the bulk target, and the composition was little affected by the applied P_{O_2} ranging from 1 to 9 Pa. However, the formed grain size dramatically decreased with increasing applied P_{O_2}. The average sizes are estimated to be around 200 nm for 1 Pa, 100 nm for 5 Pa and 50 nm for 7 Pa, as shown in Fig. 7. The reason seems to be that increasing P_{O_2} reduced the grain mobility to form accumulated large grains on substrates. In this experiment, no obvious grain shape was observed for P_{O_2} of 9 Pa. Under the present experimental conditions, therefore, lower P_{O_2} is advantageous for preparing SBN thin films with relatively large grains that have a potential for exhibiting

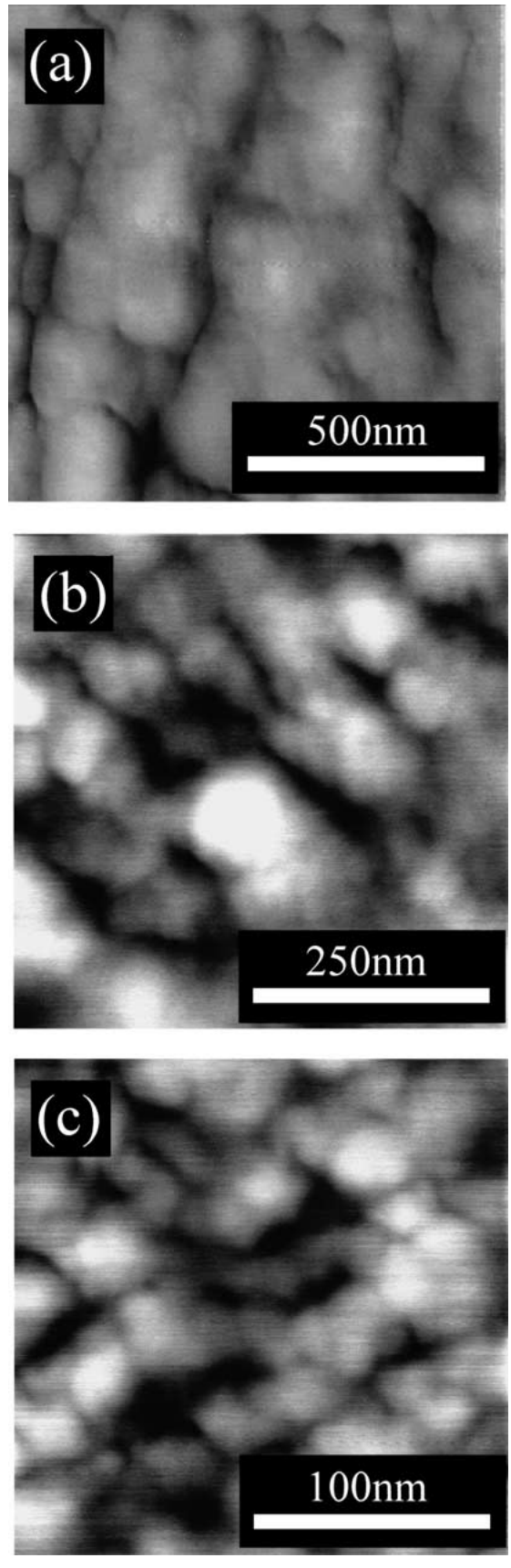

Figure 7 AFM images of $Sr_{0.3}Ba_{0.7}Nb_2O_6$ thin films under different oxygen partial pressure of (a) 1 Pa, (b) 5 Pa and (c) 7 Pa during PLD processing.

large P_r values. However, a slight color change from half-transparency into dark brown was observed for the thin films fabricated by lowering P_{O_2}. This seems to be caused by oxygen deficiency from its stoichiometric composition, thereby requiring post-annealing

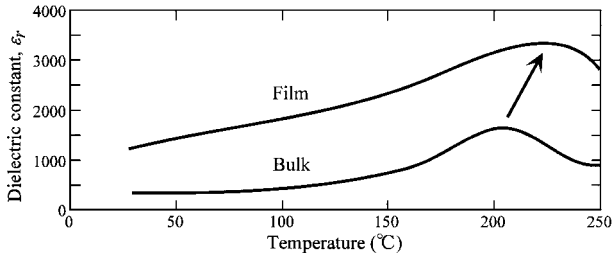

Figure 8 Comparison of temperature dependence of dielectric constant ε_r at 1 kHz for the $Sr_{0.3}Ba_{0.7}Nb_2O_6$ thin film with that for the bulk target shown in Fig. 3.

treatment under a high pressurized oxygen ambient of 2 kgf/cm^2 which resulted in reduction of a leakage current density of the film. A similar PLD condition dependence, i.e., laser flux, Po_2 and T_{sub} on the film characteristics was also observed in the processing of the other SBN thin films with x of 0.4, 0.5 and 0.6.

When Pt-coated Si substrates were used for SBN thin film deposition, it was observed that average grain sizes of the deposited films were approximately 1.5 times larger than those deposited on quartz substrates. In the case of SBN thin films with x of 0.3, an average grain size of the film deposited at Po_2 of 1 Pa was estimated to be around 300 nm. Moreover, the film demonstrated a highly preferential c-axis orientation (Fig. 2b). Highly textured c-axis orientation is required to optimize the ferroelectric properties of the films, since the c-axis is the orientation of spontaneous polarization for TTB-structured SBN. Fig. 8 compares the temperature dependence of ε_r at 1 kHz for the SBN thin film ($x = 0.3$) with that for the bulk ceramics used as a target source. It is obvious that a highly preferential c-axis orientation allows high ε_r for the thin film at all temperatures investigated. The film shows a maximum ε_r of 3500, which is much larger than 1500 for the bulk target having a random TTB orientation. Further, it is interesting to note that the Curie point increases from 200°C for the bulk target to 230°C for the film. This difference seems to be explained on the basis of microstructural differences in the bulk target and thin film, which is mentioned in the previous section, but at present, we are unable to give any qualitative explanation for the present experimental result. Fig. 9 shows a rhomboidal P–E hysteresis loop for the c-axis oriented SBN thin film with x of 0.3. The P_r and E_c of this film were measured to be 3.1 μC/cm^2 and 12.8 kV/cm, respectively. Much larger P_r and much smaller E_c values could be obtained for the c-axis oriented thin film than those for its polycrystal bulk target with a random TTB orientation shown in Fig. 6 ($x = 0.3$). The other SBN thin films with x of 0.4, 0.5 and 0.6 also demonstrated preferential c-axis orientation in their structures under appropriate deposition parameters, which resulted in a much higher dielectric constant than polycrystalline bulk ceramics.

3.3. SBN multi-layered films

A capacitance (C) of dielectric materials consisting of multi-layers is expressed as

$$C = S/(d_1/\varepsilon_1 + d_2/\varepsilon_2 + \cdots + d_n/\varepsilon_n) \quad (n = 1, 2, 3, \ldots) \tag{1}$$

where S, d_n and ε_n are the contact area, thickness and dielectric constant of each dielectric layer, respectively. Accordingly, an overall dielectric constant (ε_{all}) of multi-layered materials is also a function of the dielectric constant and thickness of each layer, and can be obtained from the following equation:

$$\varepsilon_{all} = C(d_1 + d_2 + d_3 + \cdots + d_n)/S \quad (n = 1, 2, 3, \ldots) \tag{2}$$

As shown in Fig. 3, the temperature dependence of dielectric constant (ε_r) for SBN changes widely depending on the x value. In the ferroelectric TTB region ($x = 0.3$, 0.4, 0.5 and 0.6), each of curves has a hump with a maximum peak (the Curie point), and the peak continuously shifts in the range from 50 to 250°C by controlling the x value. In order to modify the temperature (T) dependence of ε_r for many purposes, a multi-layered structure is considered to be one of the best procedures. For instance, linear or constant ε_r–T relationships in a wide temperature region are expected for micro-sensor device applications, in particular, as heat-resistant dielectric thin films compatible with a semiconductor processing for Si-based integrated circuits.

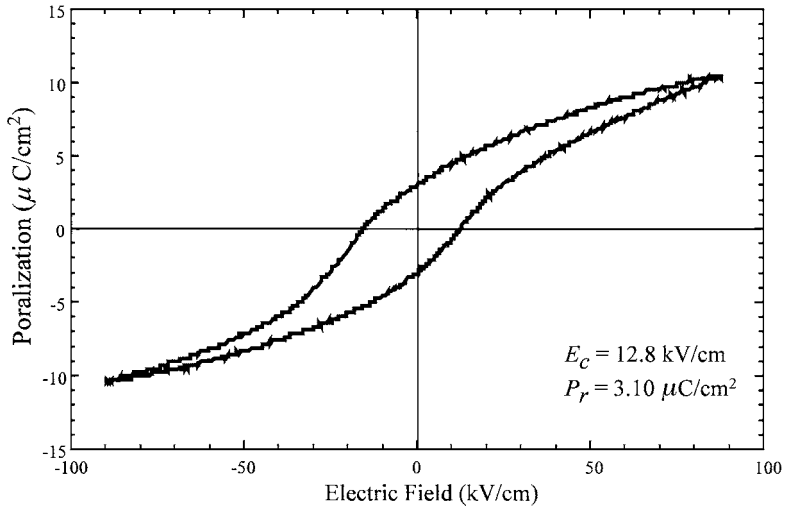

Figure 9 P–E hysteresis loops recorded at room temperature for the $Sr_{0.3}Ba_{0.7}Nb_2O_6$ thin film.

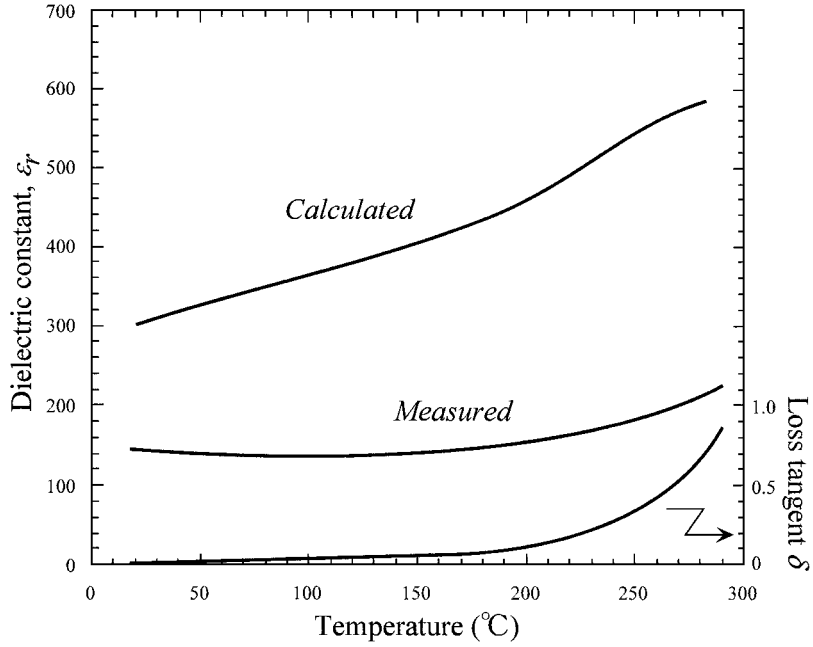

Figure 10 Temperature dependence of dielectric constant ε_r and loss tangent (tan δ) measured at 1 kHz for the multi-layered $Sr_xBa_{1-x}Nb_2O_6$ film ($x = 0.3/0.4/0.5$). The theoretical curve calculated by Equations 1 and 2 is also shown for comparison.

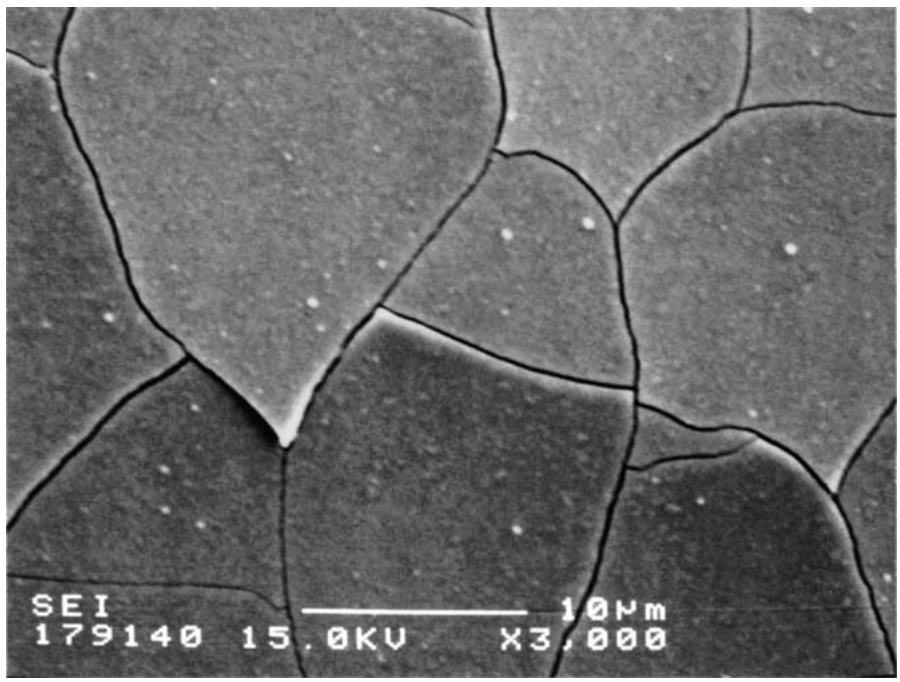

Figure 11 Surface morphology of the multi-layered $Sr_xBa_{1-x}Nb_2O_6$ film ($x = 0.3/0.4/0.5$).

In this study, multi-layered SBN films were prepared from the selected TTB-structured SBN bulk sources with x of 0.3, 0.4 and 0.5 using PLD techniques with a rotation-type multi target holder. Film deposition on a Pt/Si substrate was carried out in order of increasing x value from 0.3 to 0.5. The deposition parameters for each film were the same as those for the single film deposition, and the thickness of each deposited layer was fixed to 1 μm. Fig. 10 shows the $\varepsilon_r(T)$ and dielectric loss (tan $\delta(T)$) curves of the synthesized multi-layered SBN film. The $\varepsilon_r(T)$ and tan $\delta(T)$ curves were recorded at 1 kHz during a heating run from room temperature to around 300°C. For comparison, a theoretical $\varepsilon_r(T)$ curve calculated by Equations 1 and 2 using dielectric constant data of single-layered film specimens is also plotted in this figure. The calculated ε_r monotonically increases with increasing temperature, indicating a positive ε_r–T relationship during the entire range of temperature. On the other hand, the synthesized multi-layered SBN film shows a ε_r value at room temperature equal to half that of the calculated data, and keeps an almost constant ε_r value up to around 200°C, followed by a gradual increase at higher temperature. Tan δ also starts to increase abruptly above 200°C, and approaches 1.0, which resulted in that dielectric constant measurements became unstable at higher temperatures.

The deviation from the theoretical value in the ε_r measurement and an enormous increase in the dielectric

loss at high temperature for the synthesized multi-layered SBN film seems to be due to defects in the microstructure. Prior to the ε_r–T relationship measurement, the multi-layered SBN film was subjected to an oxygen annealing treatment at 800°C in the same way as for the single-layered film specimens. After the annealing treatment, several cracks were observed in the limited area on the surface of the multi-layered SBN film (Fig. 11), while no crack was observed in the single-layered film specimens. Mismatch in the thermal expansion coefficients among deposited thin-film layers is considered to involve stress generation and accumulation at the film/film interface during multi-deposition or annealing processes, which partially resulted in crack propagation in the film structure. According to Equations 1 and 2, the dielectric constant of multi-layered structure is determined by the dielectric constant and thickness of each deposited layer. These equations never describe a deposition order of film layers on substrates. As a matter of fact, the thermal expansion and its matching property among multi-layers, which seem to be greatly affected by each film thickness, also should be a key factor for the permittivity property of multi-layered film structure. This is one of the subjects to be further examined for preparing multi-layered films with a variety of desired ε_r–T relationships.

4. Conclusion

$Sr_xBa_{1-x}Nb_2O_6$ (SBN) thin films have the potential for use as ferroelectric memory and sensor devices compatible with Si-based integrated circuits. In particular, SBN has the advantage of containing no toxic volatile elements such as Pb. In the present study, SBN bulk ceramics have been synthesized by pressure less sintering through a mixed-oxide process. The SBN bulk ceramics demonstrated attractive behaviors in that the Curie point shifted to lower temperature, but the corresponding maximum dielectric constant increased with increasing x value in the range from 0.3 to 0.6. This seems to meet a wide range of commercial requests for many applications by selection of the desired SBN composition. In order for the SBN thin film to meet these requests, a superior stoichiometry control as well as crystallinity control for an excellent spontaneous polarization is required. Pulsed FHG-YAG laser deposition technique (PLD) was proved to be excellent in that the composition was easily transferred from the sintered bulk target to the deposited film. YAG laser has advantages especially in running costs, easy maintenance and safety compared to excimer lasers. The PLD-derived SBN thin film with x of 0.3 on Pt-coated Si substrate demonstrated a preferential c-axis-oriented structure, thereby showing a relatively good rhomboidal P–E hysteresis loop with a remanent polarization of 3.1 μC/cm^2 and a coercive field of 12.8 kV/cm. Further, synthesis of the multi-layered SBN film was performed for the first time by the PLD technique using bulk target sources with x of 0.3, 0.4 and 0.5. We showed the possibility that the temperature dependence of the dielectric constant for SBN film can be modified by a multi-layered film structure, while improvements in deposition and heat-treatment conditions for microstructural stability are still needed to approach the theoretically calculated results.

Acknowledgements

This work was financially supported by the Next Generation of Research for the Future, Japan Society for the Promotion of Science (JSPS-RFTF 96P00105) and by a commission research grant from Tokin Co. Ltd., Japan. Part of this work was carried out by Laboratory for Developmental Research of Advanced Materials, Institute for Materials Research, Tohoku University.

References

1. K. MEGUMI, N. NAGATSUMA, Y. KASHIWADA and Y. FURUHATA, *J. Mater. Sci.* **11** (1976) 1583.
2. P. B. JAMIESON, S. C. ABRAHAMS and J. L. BERNSTEIN, *J. Chem. Phys.* **48** (1968) 5048.
3. P. V. LENZO, E. G. SPENCER and A. A. BALLMAN, *Appl. Phys. lett.* **11** (1967) 23.
4. J. B. THAXTER, *ibid.* **15** (1969) 210.
5. R. R. NEURGAONKAR and W. K. CORY, *J. Opt. Soc. Am. B: Opt. Phys.* **3** (1986) 274.
6. A. M. GLASS, *J. Appl. Phys.* **40** (1969) 4699.
7. A. A. BALLMAN and H. BROWN, *J. Cryst. Growth* **1** (1967) 311.
8. K. NAGATA, Y. YAMAMOTO, H. IGARASHI and K. OKAZAKI, *Ferroelectrics* **38** (1981) 853.
9. N. S. VANDAMME, A. E. SUTHERLAND, L. JONES, K. BRIDGER and S. R. WINZER, *J. Amer. Ceram. Soc.* **74** (1991) 1785.
10. R. R. NEURGAONKER and E. T. WU, *Mater. Res. Bull.* **22** (1987) 1095.
11. C. J. CHEN, Y. XU, R. XU and J. D. MACKENZIE, *Ceram. Trans.* **14** (1990) 211.
12. Y. S. YANG, M. K. RYU, H. J. JOO, S. H. LEE, S. J. LEE, K. Y. KANG and M. S. JANG, *Appl. Phys. Lett.* **76** (2000) 3472.
13. S. SCHWYN THÖNY, K. E. YOUDEN, J. S. HARRIS, JR. and L. HASSELINK, *ibid.* **65** (1994) 2018.
14. W. LIN, T. TSENG, S. LIN, S. TU, S. YANG, J. HARN, K. LIU and I. LIN, *Jpn. J. Appl. Phys.* **34** (1995) L625.
15. H. CHENG, C. HU and I. LIN, *ibid.* **36** (1997) 284.
16. K. L. NGAI and T. L. REINECKE, *Phys. Rev. Lett.* **38** (1977) 74.
17. R. R. NEURGAONKAR, W. K. CORY, J. R. OLIVER, M. D. EWBANK and W. F. HALL, *Opt. Eng.* **26** (1987) 392.

Received 18 January 2001
and accepted 13 February 2002